ARCHIVES OF ELECTRICAL ENGINEERING VOL. 65(2), pp. 235-248 (2016)

DOI 10.1515/aee-2016-0016

Generalized space vector control for current source inverters and rectifiers

J. ANITHA ROSELINE, M. SENTHIL KUMARAN, V. RAJINI

SSN College of Engineering
Department of Electrical and Electronics Engineering
Chennai, TamilNadu, India
e-mail: anithar@ssn.edu.in

(Received: 27.08.2015, revised: 15.10.2015)

Abstract: Current source inverters (CSI) is one of the widely used converter topology in medium voltage drive applications due to its simplicity, motor friendly waveforms and reliable short circuit protection**.** The current source inverters are usually fed by controlled current source rectifiers (CSR) with a large inductor to provide a constant supply current**.** A generalized control applicable for both CSI and CSR and their extension namely current source multilevel inverters (CSMLI) are dealt in this paper. As space vector pulse width modulation (SVPWM) features the advantages of flexible control, faster dynamic response, better DC utilization and easy digital implementation it is considered for this work. This paper generalizes SVPWM that could be applied for CSI, CSR and CSMLI. The intense computation involved in framing a generalized space vector control are discussed in detail. The algorithm includes determination of band, region, subregions and vectors. The algorithm is validated by simulation using MATLAB /SIMULINK for CSR 5, 7, 13 level CSMLI and for CSR fed CSI.

Key words: current source rectifiers (CSR), current source inverters (CSI), current source multilevel inverter (CSMLI), space vector pulse width modulation (SVPWM)

1. Introduction

The inverters used in medium voltage can be classified as voltage source inverter (VSI) and current source inverter (CSI). As CSI features the advantage of simple converter topology with the absence of freewheeling diodes compared to voltage source inverters, reliable short circuit protection and an inherent four quadrant operation it is best suited for applications such as pumps, fans, conveyors, cranes and transportation drive systems where DC distribution network is available. In practice CSI are generally fed by a current source rectifier (CSR) as shown in Fig. 1 which improves the input power factor, reduces the line current distortion and ensures superior dynamic response. The CSR normally requires a three phase filter capacitor at its input which assists the commutation of the switching devices and to filter out line current harmonics. The major drawback of CSR fed CSI is due to the inductor used to produce a con-

stant current, which increases the conduction losses and hence reduce the efficiency of energy storage compared to capacitors in VSI. This major drawback of the inductor usage is overcome by the development of super conducting energy storage technology. An extensive survey of different topologies of a current source converter for industrial medium-voltage drives are done by the researchers. [3, 4, 7, 10-11]. The power rating of the CSI fed drive can be increased by operating two or more CSI in parallel also called as multilevel inverters (MLI). The commonly used control schemes applied for CSI are trapezoidal modulation (TPWM), selective harmonic elimination (SHE) and space vector modulation (SVM). Carrier phase shifted SPWM and trapezoidal PWM methods are applied for three phase current source inverters [5-6]. The SVM control scheme is dealt in this paper as it features the advantages such as the lowest DC current utilization due to its bypass operation and fast dynamic response. Space vector technique for DC current balance control in CSI and front end rectifiers are also studied by researchers [8, 10]. A review of analysis and simulation of multilevel inverters, dual current source inverters are also discussed for high power industrial applications [2, 9, 12-14]. A detailed mathematical computations involved in framing a space vector algorithm for multilevel cascaded voltage source inverters is investigated [1]. The SVPWM of VSI cannot be used for CSI as the current vectors are phase shifted by 30° with respect to voltage vectors. The paper is organized as, section 2 describing the power circuit and the switching states of the CSMLI topology followed by the detailed mathematical analysis of the generalized space vector approach in section 3. In section 4, the performance of the algorithm is validated by simulation using MATLAB/SIMULINK and section 5, concludes the paper indicating a certain drawback of the algorithm.

2. Description of the power circuit and its switching states

Figures 1 and 2 show the power circuit of CSR and CSMLI considered for this work. The CSMLI topology is composed of two three-phase CSI modules connected in parallel. The power rating and the level can be increased by connecting N three phase modules in parallel. The inverter is assumed to be fed from an ideal current source. In practice it is obtained using current source rectifier as shown in Fig. 1 with a large inductor to provide a constant supply current. Three phase capacitor C_f at its output as shown in Fig. 2 is required to assist the commutation of the switching devices. It also acts as a harmonic filter and eliminates the high dv/dt problem. The switching states of the CSI are valid provided it satisfies the following constraint.

1) Only 2 switches in each modular unit should conduct at any time instant, one in the top half and other in the bottom half.
2) Minimum number of switching is required when I_{ref} transfers from one region to the other.

Based on this constraint the inverter has a total of 81 switching states which are further identified as 66 active and 15 zero states. The On-State Switches of the modular units are shown in Table 1.

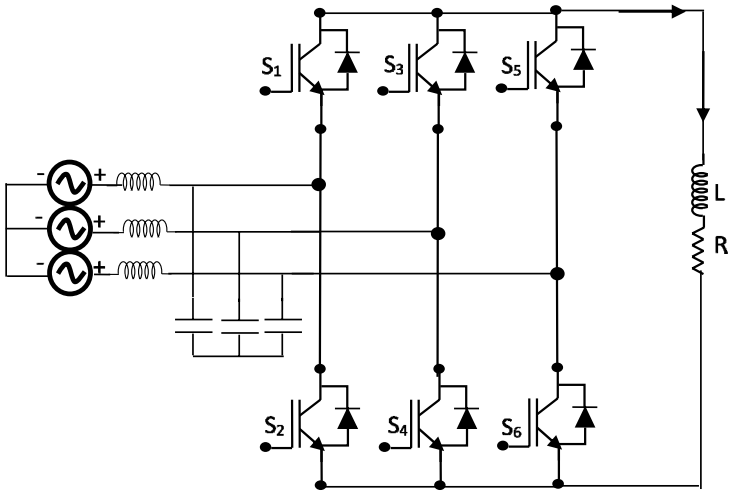

Fig. 1. Topology of current source rectifier

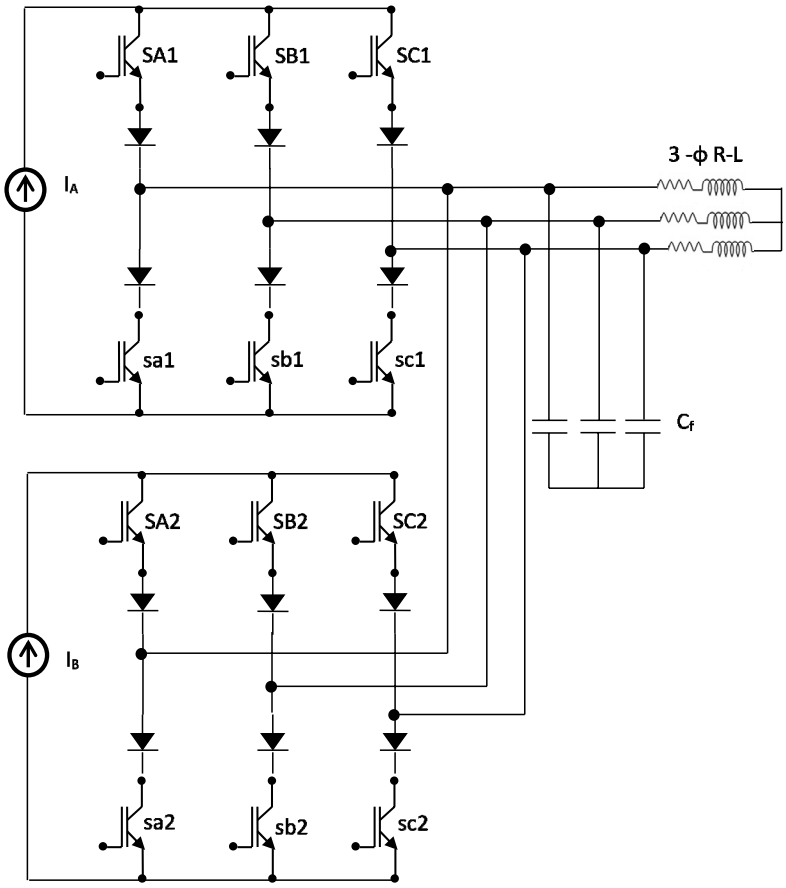

Fig. 2. Modular topology of 5 level current source inverter

Table 1. Switching states of a 5 level CSMLI

Type	On-State Switches- Top unit	On-State Switches- Bottom unit
Zero States	SA1,sa1	SA2,sa2
	SB1,sb1	SB2,sb2
	SC1,sc1	SC2,sc2
Active States	SA1,sb1	SA2,sb2
	SA1,sc1	SA2,sc2
	SB1,sc1	SB2,sc2
	SB1,sa1	SB2,sa2
	SC1,sa1	SC2,sa2
	SC1,sb1	SC2,sb2

3. Mathematical analysis

Figure 3 shows the major steps involved in framing the control algorithm to generate the switching pulses. The algorithm is developed assuming that the DC current sources are stable and the operation is balanced.

3.1. Generation of current space vectors

Assuming that the operation of the inverter is balanced. The instantaneous three phase output currents I_{an}, I_{bn}, I_{cn} of phase *A, B* and *C* is given by (1)

$$I_{an}(t) + I_{bn}(t) + I_{cn}(t) = 0 \tag{1}$$

The three phase currents (I_{abc}) are transformed to 2D plane (α, β) using Clarke's transformation. The current space vectors corresponding to any state of parallel inverter can be obtained using (2) and (3)

$$I_S(t) = I_{an}(t) + I_{bn}(t)e^{-i\frac{2\pi}{3}} + I_{cn}(t)e^{-i\frac{2\pi}{3}}, \tag{2}$$

$$I_S(t) = i_\alpha(t) + i_\beta(t), \tag{3}$$

where

$$i_\alpha = I_{an} + I_{bn}\cos\frac{2\pi}{3} + I_{cn}\cos\frac{4\pi}{3},$$

$$i_\beta = I_{bn}\sin\frac{2\pi}{3} + I_{cn}\sin\frac{4\pi}{3}.$$

The space vector plot can be obtained by plotting α vs. β. The vector patterns obtained for 5 and 7 level current source multilevel inverters are shown in Fig. 4.

From Fig. 5, it can be observed that the space vectors forms hexagonal pattern for both CSI and VSI MLI, which are further divided into 6 major regions (R_1-R_6) but current vectors are phase shifted by 30° with respect to voltage vectors. Hence SVPWM of voltage source inverters cannot be used for current source converters. As the vector plots of CSI and CSR are identical and CSMLI are extensions of CSI the algorithm is unified.

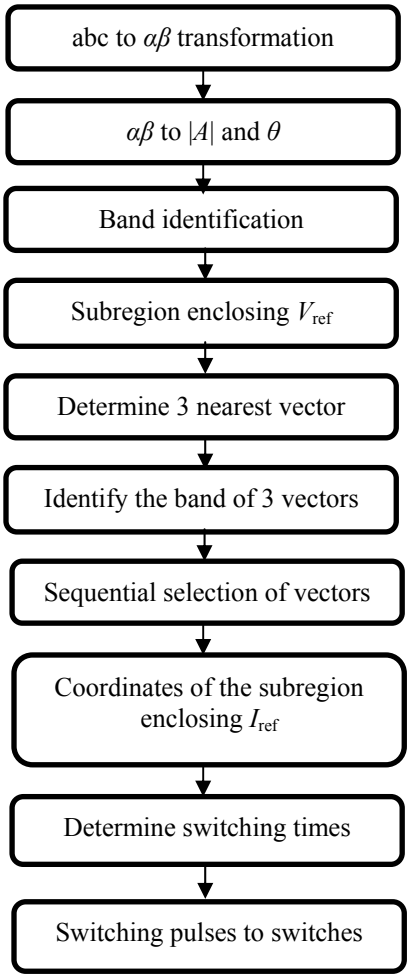

Fig. 3. Flow chart of the algorithm

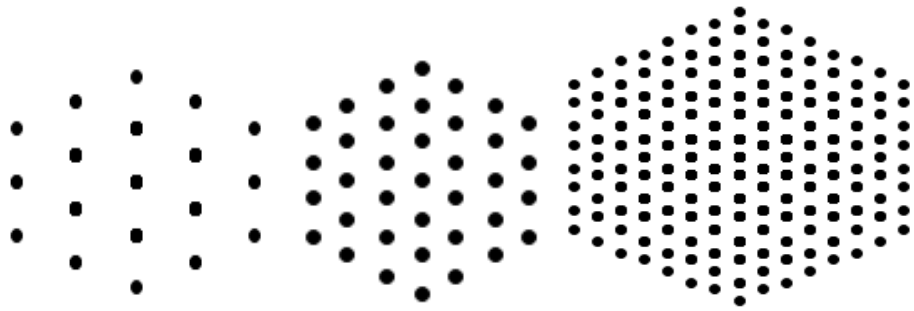

Fig. 4. Space vector distribution for 5, 7 and 13 level CSMLI

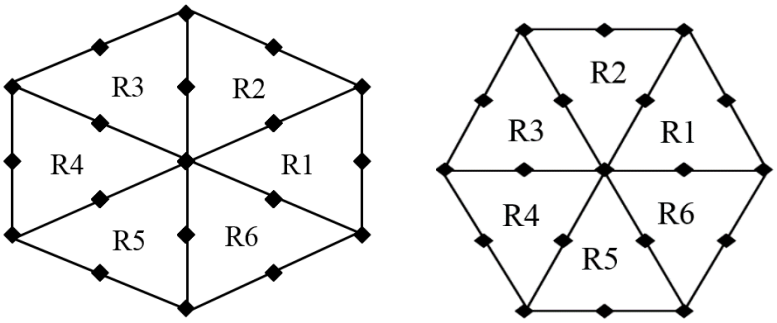

Fig. 5. Space vector pattern of CSI and VSI

3.2. Determination of magnitude ($|A|$) and theta (θ)

The location of the reference vector I_{ref} is determined based on $|A|$ and θ as described below. Having found α and β using (4) and (5), magnitude and theta can be calculated as

$$|A| = \sqrt{\alpha^2 + \beta^2}\ , \tag{4}$$

$$\theta = \tan^{-1}\left(\beta / \alpha\right). \tag{5}$$

3.3. Determination of band (B)

The space between hexagons formed by the vectors is defined as band (B). Band is also designated as a layer in the literature. From Fig. 6 it can be observed that the number of hexagons (H) is proportional to the number of bands, (6) gives the generalized relationship between B and level (N) of the inverter.

$$H = B = N - \frac{N-1}{2}, \tag{6}$$

If = 5, $B = H = 3$ as shown in Fig. 6a.

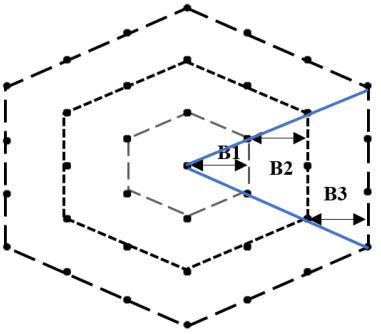

Fig. 6a. Bands of 5 level CSI

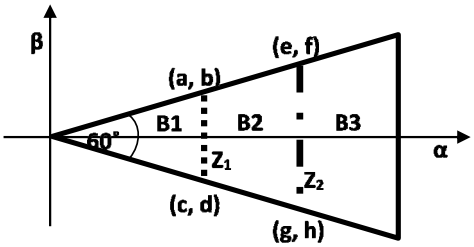

Fig. 6b. Enlarged view of R_1

Magnitude $|Z_m(t)|$ and theta $\angle Z_m(t)$ of the dotted lines as shown in Fig. 6b. Assuming the coordinate points of the lines Z_1 and Z_2 as (a, b), (c, d), (e, f) and (g, h) in the complex plane, the generalized equation of the dotted lines irrespective of the level is given by (7)

$$Z_m(t) = ((1-t)(p+jq)) + t(r+js) \quad \text{for} \quad (-\frac{\pi}{6} < \angle Z_m(t) < \frac{\pi}{6}), \tag{7}$$

where: $m = 1,2,...,(B-1)m$, $p = (a,e,...)$, $q = (b,f,...)$, and $s = (d,h,...)$ are the coordinate points.

Considering a five level inverter, the coordinate points and the equation of the line Z_1 were found to be

$$(a,b) = (\sqrt{\tfrac{3}{4}}, \tfrac{1}{4}) \text{ and } (c,d) = (\sqrt{\tfrac{3}{4}}, \tfrac{-1}{4}),$$

$$Z_1(t) = 0.433 + j(0.266 - 0.52t).$$

Based on the magnitude and theta of $Z_1(t)$ the band can be identified as B_1/B_2 if it satisfies the following condition given by (8)

$$\left.\begin{array}{l} if\,|I_{abc}(t)| \le |Z_m(t)|,\ B_1 \\ if\,|I_{abc}(t)| > |Z_m(t)|,\ B_2 \end{array}\right\} \text{ for } \quad (-\frac{\pi}{6} < \angle Z_m(t) < \frac{\pi}{6}). \tag{8}$$

3.4. Identification of the co-ordinates and its subregions

From the space vector pattern it is evident that the region enclosed by the reference vector forms an equilateral triangle. It is known that the sides of an equilateral triangle are the same and the height of the equilateral triangle is $\sqrt{3}/2$.

Considering triangle ABC in Fig. 7. Having known two coordinates of the triangle the third coordinate can be found by applying the sine rule. It is evident from the vector distribution that at any instant of time the reference vector is enclosed by three vectors which form a subregion (*SR*). Due to uniform distribution of the vectors the *SR* so formed are equilateral triangles. The number of *SR* increases with band and is given by (9)

$$SR = [B + (B-1)]. \tag{9}$$

To exactly identify the three nearest vectors enclosing the rotating reference vector the equation of the lines (Z_1, E_1 and E_2) as shown in Fig. 8a and hence the magnitudes with respect to theta has to be determined. Using (7), E_1 and E_2 were found to be

$$(a,b) = (\sqrt{\tfrac{3}{4}}, \tfrac{1}{4}), (\sqrt{\tfrac{3}{4}}, \tfrac{-1}{4}) \text{ and } (c,d) = (\sqrt{\tfrac{3}{4}}, 0),$$

$$E_1(t) = 0.433(1+t) + j(0.266 - 0.266t) \quad for \quad (0^o < \angle Z_m(t) < 30^o),$$

$$E_2(t) = 0.433(1+t) - j(0.266 - 0.266t) \quad for \quad (-30^o < \angle Z_m(t) < 0^o).$$

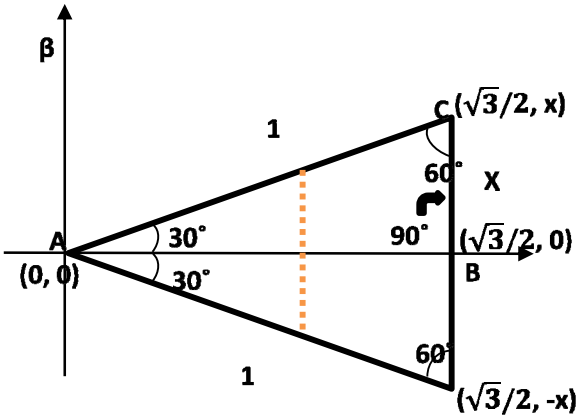

Fig. 7. Determination of co-ordinates

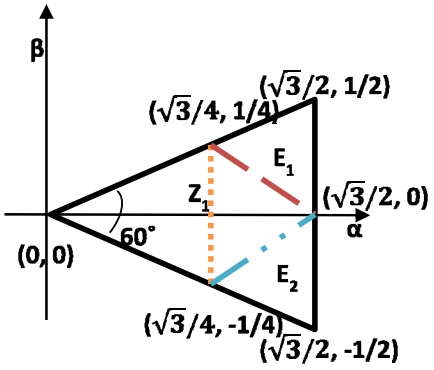

Fig. 8a. Co-ordinates of R_1

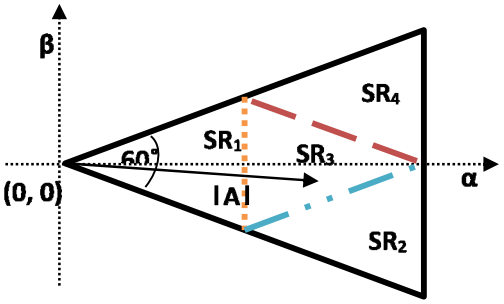

Fig. 8b. Identification of subregions

Having found the equations of the lines Z_1, E_1, E_2 the location of the reference vector can be identified as SR_1 to SR_4 based on the constraints as follows

$$\text{If } |A| < |Z_1| \text{ and } B = 1 \text{ and } (\frac{-\pi}{6} < \theta < \frac{\pi}{6}) \text{ then } SR_1,$$

$$\text{If } |A| < |E_2| \text{ and } B = 2 \text{ and } (\frac{-\pi}{6} < \theta < 0) \text{ then } SR_3,$$

$$\text{If } |A| > |E_2| \text{ and } B = 2 \text{ and } (\frac{-\pi}{6} < \theta < 0) \text{ then } SR_4,$$

$$\text{If } |A| < |E_1| \text{ and } B = 2 \text{ and } (0 < \theta < \frac{\pi}{6}) \text{ then } SR_3,$$

$$\text{If } |A| > |E_1| \text{ and } B = 2 \text{ and } (0 < \theta < \frac{\pi}{6}) \text{ then } SR_2.$$

3.5. Selection of vectors

To minimize the harmonic distortion and number of switching per sample, the nearest three vectors and its corresponding band has to be selected. Fig. 9(a-c), the selection of three nearest vectors in R_1 is explained and its extension to the other regions are explained in Fig. 10. In Fig. 9a, it can be observed that numbers are assigned to each subregions within a region which are again normalized in Fig. 9b to enhance easy computation. The normalized subregions are further scaled down to 1 and 0 in Fig. 9c, where 0 denotes odd numbered triangles and 1 denotes even numbered triangles to ensure the proper sequence of vector selection.

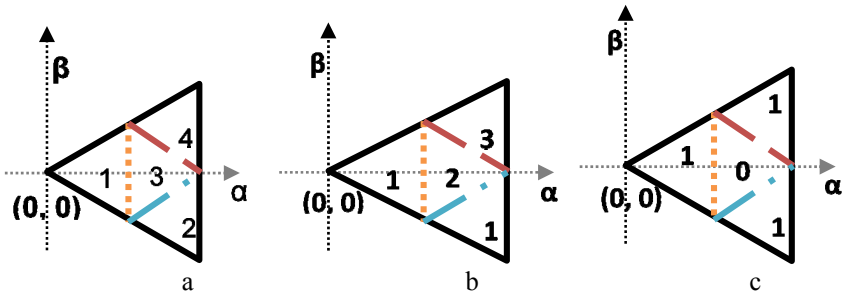

Fig. 9 (a-c). Normalization of sub regions in R_1

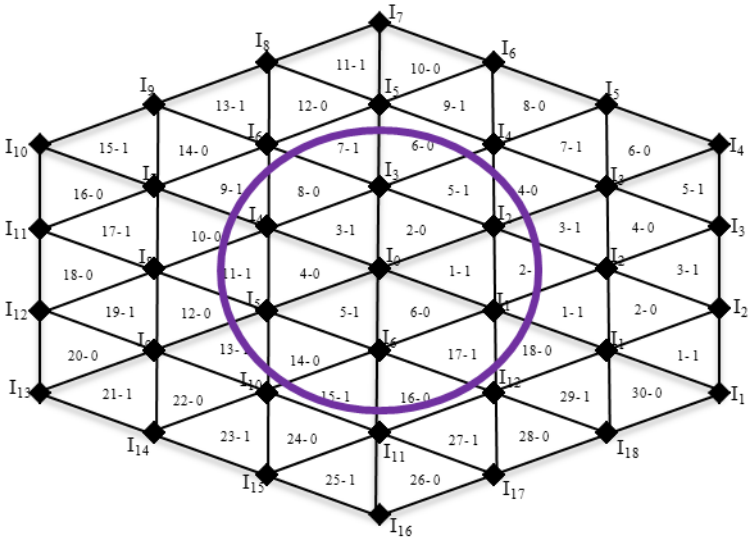

Fig. 10. Normalization applied to all regions (R_1-R_6)

Fig. 10 denotes that the reference space vector traverse through B_2 the selection of nearest three (I_1, I_2 and I_3) vectors for all regions are unified and mathematically formulated as given by (10 – 14), for an odd numbered subregion,

$$I_1 = \frac{T_{NM}}{2} + (BR-1)B\,, \tag{10}$$

$$I_3 = I_1 - (BR-1)\,. \tag{11}$$

For even numbered subregion,

$$I_1 = T_{NM} - \text{int}\left(\frac{T_{NM}}{2}\right) + (BR-1)(B-1)\,, \tag{12}$$

$$I_3 = I_1 + BR\,. \tag{13}$$

For both odd and even numbered subregions

$$I_2 = I_1 + 1\,. \tag{14}$$

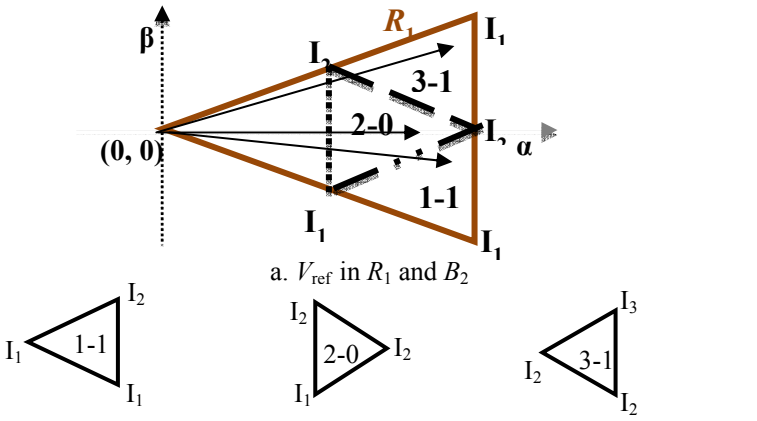

a. V_{ref} in R_1 and B_2

b. I_{ref} in R_1, B_2 and SR_1 c. I_{ref} in R_1, B_2 and SR_2 d. I_{ref} in R_1, B_2 and SR_3

Fig. 11. Selection of nearest vector in R_1

Having found the nearest three vectors, from Fig. 11 it is evident that vectors are selected from different bands of the hexagon. (15) and (16) is used to find specific bands and regions of three vectors.

For normal or odd numbered triangle,

$$\text{Band for } I_1 \text{ and } I_2 + B,\ \text{Band for } I_3 = (B-1)\,. \tag{15}$$

For inverted or even numbered triangle,

$$\text{Band for } I_1 \text{ and } I_2 = (B-1),\ \text{Band for } I_3 = B\,. \tag{16}$$

3.6. Dwell time calculation

For a sampling period Ts, the dwell time for the nearest three vectors represents the duty cycle time of the chosen switches. The dwell time calculation is based on an ampere-second

balancing principle. The ON time of the switches depend on the duty cycle of three switching vectors. From Fig. 12 by vector addition to synthesize reference voltage, (17) must be satisfied. Solving (18), (19) and (20) D_1, D_2 and D_3 can be determined.

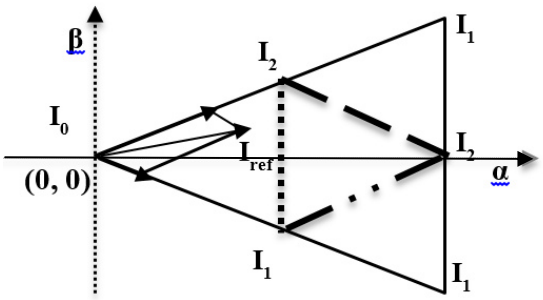

Fig. 12. Synthesis of reference vector I_{ref}

$$D_1 I_1 + D_2 I_2 + D_0 I_0 = I_{\text{ref}}. \tag{17}$$

This implies that

$$D_1 X_1 + D_2 X_2 + D_0 X_0 = 0, \tag{18}$$

$$D_1 Y_1 + D_2 Y_2 + D_0 Y_0 = 0, \tag{19}$$

where D_i is a duty cycle and X_i, Y_i are co-ordinates of I_i with reference to I_{ref} (where $i = 1, 2, 3$) and since I_1, I_2 and I_3 encloses I_{ref}.

$$D_1 + D_2 + D_0 = 1. \tag{20}$$

Modulation index (m_a) for CSI is given by (21)

$$m_a = \frac{I_{\text{ref}}}{I_d}, \tag{21}$$

where $I_{ref(max)} = I_d$ and $m_{\max} = 1$.

The range of m_a is $0 \le m_a \le 1$.

4. Simulation results

The performance of the proposed algorithm technique has been validated by simulation in the MATLAB/SIMULINK environment for 5, 7, 13 level CSI-MLI current source rectifier and 3 φ CSR fed CSI with RL load. The simulation parameters are shown in Table 2.

Fig. 13 is the load voltage and load current waveforms obtained for 5 level CSMLI. The CSMLI comprises of two modules of CSI connected in parallel. Each modules are fed by ideal

current source of 1 A. At modulation index $m_a = 0.7$, $V_{\text{ph (peak)}} = 39.8$ V, $V_{L\text{ (peak)}} = 68.9$ V, $I_{L\text{ (peak)}} = 2$ A, $I_{L\text{ (rms)}} = 1.414$ A.

Table 2. Simulation Parameters of 7 level CSI MLI

Quantity	Value
R-L Load	$R = 20\Omega$, $L = 27$ mH
Ideal current source	5 A (5 level)
Output voltage frequency	50 Hz
Switching frequency	5 kHz

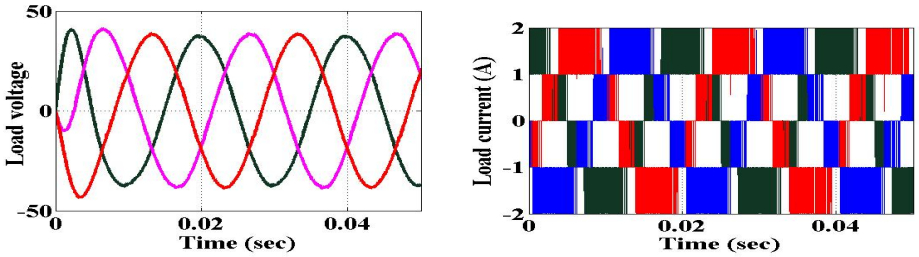

Fig. 13. Load voltage and load current waveforms of 5 level CSI-MLI

In Fig. 14 the load voltage and load current waveforms obtained is shown by incorporating the algorithm for 7 level CSMLI. The CSMLI comprises of three modules of CSI connected in parallel. Each modules are fed by ideal current source of 5A. At modulation index $m_a = 0.9$, $V_{\text{ph (peak)}} = 333$ V, $V_{L\text{ (peak)}} = 576.77$ V, $I_{L\text{ (peak)}} = 15$ A, $I_{L\text{ (rms)}} = 10.6$ A.

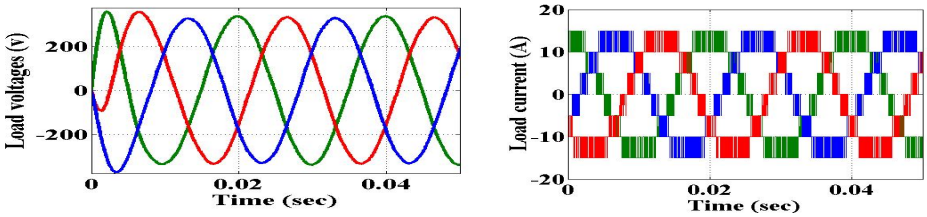

Fig. 14. Load voltage and load current waveforms of 7 level CSI-MLI

The load voltage and load current waveforms obtained by incorporating the algorithm for 13 level CSMLI is shown in Fig. 15. The CSMLI comprises of three modules of CSI connected in parallel. Each modules are fed by ideal current source of 2 A, 4 A and 8 A. At $m_a = 0.86$, $V_{\text{ph (peak)}} = 282$ V, $V_{L\text{ (peak)}} = 488.43$ V, $I_{L\text{ (peak)}} = 12$ A, $I_{L\text{ (rms)}} = 8.48$ A.

The proposed algorithm has also been applied for a current source inverter fed by a current source rectifier. The rectifier output voltage and current obtained when operated at unity modulation index are shown in Fig. 16. The line $V_{ab} = 77$ V, phase voltages $V_{bn}=V_{cn} = 46$ V of current source inverter fed by CSR are shown in Fig. 17.

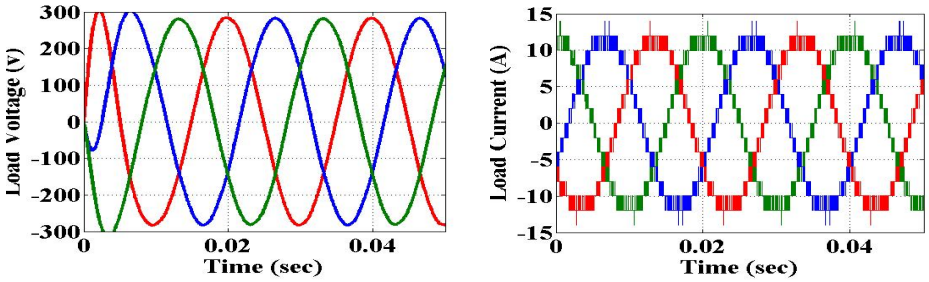

Fig. 15. Load voltage and load current waveforms of 13 level CSI-MLI

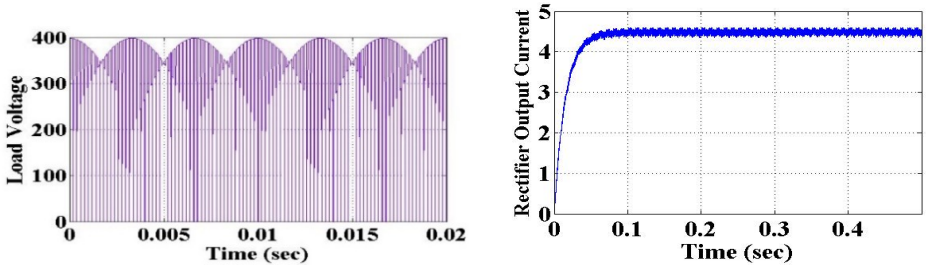

Fig. 16. Load voltage and load current waveforms of current source rectifier

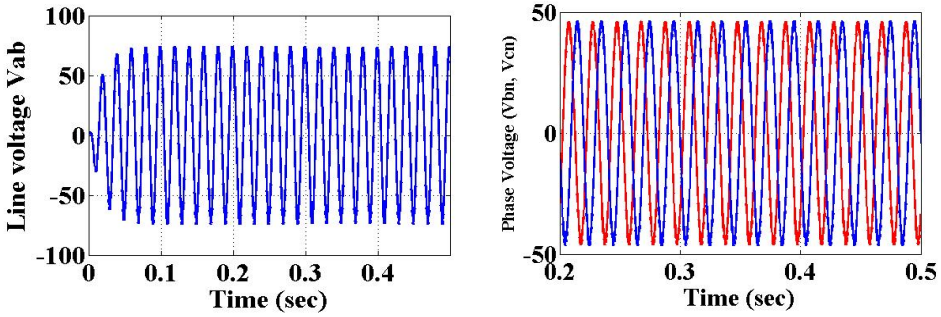

Fig. 17. Line voltage V_{ab} and phase voltage V_{bn} and V_{cn} of CSR fed CSI

Table 3. Analysis of THD and fundamental component of load voltage and current

Total Harmonic Distortion Analysis			**Fundamental (50)Hz**		m_a
	Load Voltage	Load Current	Load Voltage	Load Current	
5 level CS-MLI	1.45%	37.62%	37.82	1.6	0.6
7 level CS- MLI	1.14%	19.93%	334.9	14.22	0.9
13 Level CS-MLI	0.66%	9.04%	282.9	12.01	0.86

A comparative analysis of total harmonic distortion and fundamental components of load current and load voltage at specific modulation indices are studied for 5, 7 and 13 level current

source multilevel inverters as shown in Table 3. It can be observed from the table that the THD of both current and voltage reduces with increase in level which marks the advantage of higher level inverters.

5. Conclusion

A generalized approach to employ space vector pulse width control technique for current source rectifiers, inverters and multilevel current source inverters was proposed. The perplexity involved in framing the algorithm is discussed in detail. The developed control is validated by simulation using Matlab/Simulink. The simulation result proves that it can be employed to any type and level of parallel inverters and rectifiers. A comparison among different levels of CSMLI has also been done. The major drawback of this method is that it cannot be applied when the system is unbalanced.

References

[1] Johnson R.A, Rajini V., Vijayenthiran S., Kumaran M.S, *2D Digital Vector Control Algorithm for Cascaded Multilevel Converters*, Australian Journal of Basic and Applied Sciences, 8(18): 195-206 (2014).

[2] Palaniappan R., Vithayath J., Datta S. K., *Principle of a Dual Current Source Converter for AC Motor Drives*, IEEE Transactions on Industry Applications, 8IA-15(4): 445-452 (1979).

[3] Antunes F. L. M., Braga A. C., Barbi I., *Application of a Generalized Current Multilevel Cell to Current-Source Inverters*, Proc. Int. Conf. Industrial Electronics, Control, and Instrumentation, IEEE, 278-283 (1995).

[4] Xiong Y., Chen D., Yang X., Hu Ch., Zhang Zh., *Analysis and Experimentation of A New Three-Phase Multilevel Current-Source Inverter*, Power Electronics Specialists Conference, 56-62 (2004).

[5] Xu D., Wu B., *Multi-Level Current Source Inverters with Phase-Shifted Trapezoidal PWM*, Power Electronics Specialists Conference, 251-259 (2005).

[6] Bai Zh., Zhang Zh., Zhang Y., *A Generalized Three-Phase Multilevel Current Source Inverter with Carrier Phase-Shifted SPWM*, Power Electronics Specialists Conference, 104-110 (2007).

[7] Wu B., Pontt J., Rodriguez J., Bernet S., Kouro S., *Current Source Converter and Cycloconverter Topologies for Industrial Medium- Voltage Drives*, IEEE Transactions on Industrial Electronics, 7(55): 2786-2797 (2008).

[8] Li Y. W., Wu B., Xu D., Zargari N. R., *Space Vector Sequence Investigation and Synchronization Methods for Active Front End Rectifiers in High Power Current Source Drives*, IEEE Transactions on Industrial Electronics, 55(3): 1022-1034 (2008).

[9] Dawley R., Bhattacharya S., *Control of Multi Level Three Phase Dual Current Source Inverters for High Power Industrial Applications*, Industry Applications Society Annual Meeting, 4-8 (2009).

[10] Marek Adamowicc., MarcinMorawiec., *Advances in CSI-fed Induction motor drives,* Proc. Int. Conf. Compatability and Power electronics, Tallinn, Estonia, 1-7 (2011).

[11]Rabkowski J., Zdanowski M., Nowak M., Barlik R., *Fault Protection system for Current Source Inverter with Normally on Sic JFETs,* Materials Science Forum, 750-753, (2011).

[12] Vamsi Sree M., Reddy M. R. P., Rambabu CH., *A Novel 7-Level Parallel Current Source Inverter for High Power Application with DC Current Balance Control*, International Journal of Electronic and Communication Technology 3(4): 73-79 (2012).

[13] Miguel Pablo Aguirre., Laura Calvino., Maria Ines Valla., *Multilevel Current source Inverter with FPGA Control*, IEEE Transactions on Industrial Electronics, 1(60): 3-9 (2013).

[14] Himanshu N Chaudhari., Dhrupa M Patel., Maulik A Chaudri., *Analysis and Simulation of Asymmetrical Current Source Multilevel Inverter*, International journal of engineering sciences and research technology, 3(2): 554-558 (2014).